

# Peano modes at the D=2 delocalization transition

V. G. Benza

Dipartimento di Scienza e Alta Tecnologia, Universita' dell' Insubria, 20064 Como, Italy

PACS numbers: 82.35.Pq, 64.60.Al, 61.44.Br, 63.50.-x, 63.20.D-, 05.40.Jc

E-mail: [vincenzo.benza@uninsubria.it](mailto:vincenzo.benza@uninsubria.it)

**Abstract.** We study the relaxation of the Peano chain's deformations in the presence of gaussian noise. The D=2 spring network which models the chain's elasticity has no bulk, but only boundaries: its continuum version would be a flat and thin elastic strip covering the plane, smoothly curved so as to follow the Peano pattern.

We find normal modes, herefrom named Peano modes: in the same way as crystal waves are sustained by the matching of translations with rotations, the Peano modes correspond to the matching of  $\pi/4$  rotations with discrete dilatations. The eightfold symmetry is shared by the Peano chain with the octagonal quasicrystal, but the latter has a much higher connectivity. The relaxation process which starts from the Peano chain is found to mark the saddle point separating the solid from the liquid, the phase separation being driven by anisotropy. For the equivalent quantum mechanical problem this corresponds to the D=2 quantum delocalization transition.

Various experimental observations, regarding a priori uncorrelated systems, come together within the viewpoint proposed here, at least as far as their qualitative behavior is concerned.

1) Two features observed in experiments on D=2 colloids [1, 2] can be understood within the model: the bosonic peak occurring at low frequencies in the phononic spectrum and the time evolution and spatial structure of excitations. Excitations initially concentrated in small regions progressively expand towards structures of increasingly large size. 2) The so-called inverse energy cascade of D=2 turbulence [3].

3) The recently observed liquid to quasicrystal transition in bilayer water [4]. 4) Self-similar DNA conformations are connected here with structures lying at the boundary between a liquid and a solid, such as colloids and quasicrystals. **Submitted to: *Journ. of Statistical Mechanics: Theory and Experiment*. A short version, entitled 'Scale-free response of the D=2 globular phase' has been submitted to *Phys.Rev.Lett.* on July 27th, 2014.**

## 1. Introduction

In this work we study the harmonic spectrum and the time relaxation of the planar Peano-Hilbert curve  $PH_2$ . The Peano-Hilbert curves in  $D$  dimensions ( $PH_D$ ) find various applications in informatics, in association with the problem of ordering multidimensional data [5, 6] and in electronics for manufacturing miniature antennas [7]. In polymer physics  $PH_3$  has been proposed as a possible final state of a scale-invariant collapse [8]. Quite remarkably, given its high degree of deterministic ordering,  $PH_3$  has been found to fit with the path described in space by the chromosomal DNA in humans, over a rather large range of scales [9]. This result was obtained by detecting the physical contact frequencies between pairs of genomic loci, using chromosome conformation capture methods [10]. As regards the dynamics, significant data emerged from experiments on bacterial (E.coli) chromosomes [11, 12]. It was found that DNA loci undergo anomalous diffusion with a rather sharp distribution in the exponents, where the dominant behavior is  $t^{0.4}$ ; this subdiffusion can be associated to a fractal dimension  $D_f \leq 3$  [13]. A physical description of a structure having fractal dimension  $D_f \approx 3$  could be of some interest for cell biologists only when based on quantitative informations regarding, to say a few, the chain topology, the distribution of crosslinks, the nature of interchain interactions. The problem appears to be even harder when considering that those interactions are influenced by the complex multicomponent medium of the cell's nucleus or nucleoid.

Although originally motivated by the phenomenology mentioned above, this paper is limited to studying the general properties of harmonic models which can be defined over the geometry of Peano-Hilbert chains. We give a detailed analysis of the D=2 case, which turns out to be solvable, and briefly discuss  $PH_D$  within a mean-field approach. We consider a quasi one-dimensional elastic strip, modeled as an elastic network running along the closed  $PH_2$  curve, also known as Moore curve. By assigning an harmonic energy to the deviations from the  $PH_2$  pattern, we study the elasticity of the strip. We do that for all periodic approximants of  $PH_2$ , that are constructed on the square lattice by deterministic inflation rules. The elastic couplings introduced in the model follow the local geometry: more specifically they vary in dependence with the orientation of the links connecting nearest neighbours and with the angle formed by the links at the vertices. As a consequence of anisotropy the resulting mechanical network turns out to be rigid; in other words apart from uniform translations it does not allow for zero-energy modes. In particular rigid rotations or uniform dilatations of any portion of the network carry an energy cost. The model does not account for the interaction among physically adjacent sites when they are distant along the chain: our aim is to describe waves propagating along meandering one-dimensional patterns, not necessarily having the nature of covalent bonds. This description could as well apply to electromagnetic waves, but here we limit our attention to the elasticity of closely packed ensembles. In fact it is known that the D=2 elasticity has strong similarities with the D=2 electromagnetism: the elastic deformations can be decomposed into irrotational

and solenoidal components, where dilatation ( $\mathcal{D}$ ) and shear ( $\mathcal{S}$ ) have the roles of electric and magnetic field. The main difference between the two theories regards the wave propagation properties, because dilatation pays a higher energy with respect to shear, and as a consequence in the medium's bulk the longitudinal ( $\mathcal{D}$ ) field propagates with an higher velocity with respect to the transverse ( $\mathcal{S}$ ) field. As it is familiar to geologists, the two distinct waves couple at the medium's boundary, where they form the Rayleigh waves, which are characterized by nontrivial (boundary-dependent) dispersion laws.

This dependence on the boundary's geometry is exploited to extract information during earthquakes, but in the case of electromagnetism it can be used both to extract and to manipulate information, as done, e.g., by scattering electromagnetic waves through photonic crystals [14] or by engineering e.m. wavefronts with metamaterials. [15]. In the elastic model in question here the particular ordering enforced by the Peano pattern, which is built by inflating quadrupolar partitions of planar regions at discrete scales, produces the following quite intriguing effect: as we will illustrate, there are non-dispersive Rayleigh waves, named Peano waves. As regards the physical interpretation of our network model, it is important to recall some known facts about harmonicity versus strong coupling in high density configurations. The harmonic modeling of contact interactions among closely packed rigid disks goes under the name of fluctuation method [16]. Within this method one can give a precise meaning to the notion of contact (harmonic) network [17, 18]. The definition, as reminded in Refs. [19],[20], is the following: 'In a metastable state of a hard sphere system, two particles are considered to be in contact when they collide during some time interval  $\Delta t$  much smaller than the relaxation time of the structure, where metastability is lost, and much larger than the (thermal) collision time'. Turning to our case, if the chain's pattern is to be associated with a linear polymer, the model describes its fluctuations within a steep effective potential. Notice that the potential on its own has a time evolution, but on the larger scale of the structural relaxation. When one considers shorter times the line of minima of the potential follows the topology assigned by the ordered sequence of bendings which identify the undeformed chain. Within this polymeric interpretation, if one were to add to the picture the contact couplings among adjacent but nonsubsequent sites, one would end up with an elastic network describing a textured membrane. The phononic spectrum of such enlarged model would then display, in addition to the contributions described in this work, the behavior  $\rho(\lambda)_{D=2} \approx \lambda$  in the density of states, as expected from standard D=2 Debye spectra. It is worth mentioning at this point that some experiments on two-dimensional colloids did in fact display an anomalously high density of states at low frequencies [1, 2], superimposed to the D=2 Debye behavior. The connection of those experiments with our network model goes beyond the spectral properties, because, as it will be illustrated in the sequel, also the space-time behavior of the excitations is well described, at least qualitatively.

Here, in analogy with quasicrystals, whose phononic spectra are marked by self-similarity [21, 22, 23], we determine the spectral properties by exploiting the recursive nature of the chain. The operator in question acts on the two-dimensional space of planar

deformations; it has a  $(2 \times 2)$  block tridiagonal structure because it involves, at each chain site, the two nearest neighbours. For the sake of brevity we will call it disordered laplacian, in spite of it being neither scalar nor disordered, because the various types of vertices needed in order to describe the chain pattern are sequenced in a deterministic manner.

It turns out that in the case of  $(PH_2)$  the spectral problem for this disordered laplacian translates into a finite-dimensional trace map, which can be treated by standard methods. The phononic spectrum of the closed curve  $(PH_2)$ , known as Moore curve, is found to display a multiplicity of power-law singularities in the density of states. The exponents which characterize the singularities cover a whole interval, with a well defined smooth distribution (see Figs.5 and 6). One can get a picture of the physics implied by such an exotic spectrum by extending the analysis to the associated relaxation process, i.e. by studying the overdamped linear Langevin equation associated with the disordered laplacian. From this analysis, performed in Section 5, we obtain the following result: each singularity exponent of the spectrum identifies a class of fluctuations. The fluctuations have a scaling behavior, with respect to length (along the chain) and time, that is fully determined by the exponent itself. We then examine, in Section 6, how the anisotropy introduced in the elastic constants affects the spectrum, and find that it induces a phase separation (see Fig.7). The two phases involved, who are respectively dominated by dilatation and shear, can be identified as solid and liquid. The isotropic limit of the model corresponds to the critical point, where the two phases coalesce. At that point the interference of dilatation and shear generates, together with anomalous fluctuations, also phononic modes, the Peano modes.

If one examines the global relaxation process, one finds that the energy flows from localized to extended structures, as observed in two-dimensional colloids [1, 2] and in D=2 turbulence [3]. From the perspective of the quantum-mechanics determined by the disordered laplacian, the isotropic limit corresponds to the critical point of the D=2 quantum delocalization transition. In other words the Peano chain identifies a two-dimensional extension of the D=1 Aubry-Andre' class [24]. A liquid to quasicrystal transition has been reported for bilayer water [4] in a similar regime. A comprehensive exploration of the behavior close to the critical point should be based on the mentioned trace map; here we limit ourselves to some preliminaries regarding its symmetry properties. As illustrated in Section 7 we find an eightfold symmetry: we are thus close to the octagonal quasicrystal, but with a definitely lower connectivity. In the Conclusions we summarize our results.

Readers uninterested in the technical aspects of the work can skip Sections 2,3 and 4, and directly go over to Section 5. In Section 2 we determine the symbolic substitution rule which generates the patterns of the chain's approximants; in Section 3 we describe the mechanical model and then translate the substitution rule in terms of operators. The eigenvalue problem is finally formulated as a map for the traces of these operators. In Section 4, by means of the thermodynamic formalism for multifractals, we discuss the power law singularities found in the spectrum. The physical picture is given in Section

5: in discussing the network's relaxation we connect the spectral exponents with the scaling behavior of the fluctuations. This allows to obtain explicit formulas for the anomalous diffusion exponents and for the fractal dimensions. Section 6 is dedicated to the solid-liquid phase separation and to the relaxation process. We also discuss a mean-field argument which applies to Peano-Hilbert chains of arbitrary dimension D; in D=3 the argument seems to agree with measures of anomalous diffusion exponents performed on bacterial nucleoids [11, 12].

Section 7, where we qualitatively introduce the symmetry properties of the critical point, relies on some results regarding the D=1 delocalization transition.

## 2. Symbolic substitution rule for the closed chain

The approximant of order  $k$  of the closed Peano-Hilbert chain  $PH_2$  is a path of length  $N_k = 4^k$  (see Fig.2) with no intersections which connects all points of the  $(2^k \times 2^k)$  square lattice. Notice that two choices are available for the path orientation, because the plane is an oriented surface. Furthermore, since the plane has the topology of  $S^2$ , the path is an equator which cuts the plane into two polar regions. E.g. when the path is oriented anticlockwise, it makes a  $2\pi$  rotation around the polar region it encloses. At first sight it is equivalent to assign a model over the square lattice or over the Peano approximant, but one easily realizes that the latter assignment is topologically different. In fact the lattice has the topology of a torus while the Peano chain has the topology of a circle which separates the plane in two polar regions (see also the caption of Fig.3).

Let us now proceed to enumerate all vertices to be expected in the pattern: this is a preliminary step if one wants to identify such patterns with symbolic words. There are  $6 \times 2$  different vertices: we label them with the numerals  $n$  and  $\tilde{n}$ , ( $n = 1, 2, \dots, 6$ ); the two groups of six vertices correspond to opposite orientations, as illustrated in Fig.1. One thus represents the approximant of order  $k$  with a symbolic word  $W^k$  made out of the letters  $l$  of the alphabet defined above:

$$W^{(k)} \equiv l(N_k)l(N_k - 1)\dots\dots l(3)l(2)l(1). \tag{1}$$

This alphabet is exceedingly extended: in fact one can write every vertex as the image of a single given one (flat or orthogonal). The operations needed are the discrete rotation  $R$ , the inversions  $P_x, P_y$  with respect to the x and y axes and the path inversion  $\mathcal{T}$ . We give here a short list of the action of such operations on vertices:  $\mathcal{T}(m) = \tilde{m}$ ,  $\mathcal{T}(m(n)\dots m(1)) \equiv \tilde{m}(1)\dots\tilde{m}(n)$ ;  $P_x(\tilde{4}) = 3$ ,  $P_y(1) = \tilde{4}$ ,  $P_y(P_x(2)) = 4$ ;  $4 = R(1)$ ,  $1 = R(2)$ . We thus single out as basis elements the vertices  $m = 4$  and  $m = 6$ . Our aim is to write the substitution rule for the Peano inflation under the constraint of closed path. It is quite remarkable that the constraint is sufficient to identify the rule. In order to make this point clear, let us consider how the vertex  $m = 4$  can be inflated. Every vertex has four descendants, hence two descendants are placed at the boundary with the other portions of the chain. As exemplified in Fig.3, the pattern at the boundary can have two forms. In the absence of the closed path constraint this would

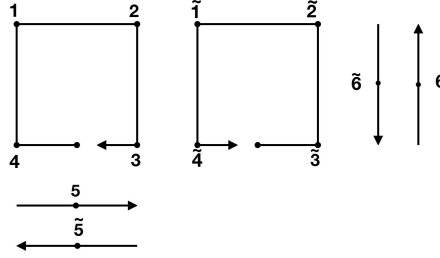


**Figure 1.** In this figure we specify the convention used for labeling the different types of vertices. As the Peano iteration is based on a quadripartite structure, in order to assign labels to vertices one can start with the elementary square-shaped closed path. Since paths can as well go through lattice sites without bending, in addition to orthogonal vertices also the flat ones (horizontal and vertical) must be accounted for. Here with the numerals (1, 2, 3, 4) and (5, 6) we respectively classify the patterns of orthogonal and flat vertices in the clockwise path; the vertices corresponding to the anticlockwise path are labeled with ( $\tilde{1}$ ,  $\tilde{2}$ ,  $\tilde{3}$ ,  $\tilde{4}$ ) and ( $\tilde{5}$ ,  $\tilde{6}$ ).

imply twofold branchings at every inflation step. Due to the periodicity requirement, as one easily verifies, this ambiguity is eliminated. It turns out that at every order only two complementary patterns are allowed. This is exemplified in Fig.3 for the first iteration: the two copies enclose the two polar regions of  $S^2$ . Along the boundary of the polar region chosen here, as shown in Fig.2, the chain's lower left quarter ( $L\mathcal{L}$ ) is connected to its lower right ( $L\mathcal{R}$ ) and upper left ( $U\mathcal{L}$ ) neighbours according to the rule specified below. The ( $L\mathcal{L}$ ) – ( $U\mathcal{L}$ ) link is vertical and placed externally, the ( $L\mathcal{L}$ ) – ( $L\mathcal{R}$ ) link is horizontal and placed internally. In summary the four quarters are connected through the two external (left and right) vertical links and the two central horizontal links: the H-shaped pattern displayed in Fig.3 (on the right side) reproduces itself at all orders. It is thus seen that the Peano chain separates the two 'polar regions' of  $S^2$  in a quite intermingled fashion. Going back to our inflation rule, the chosen convention is written as follows:  $4 \rightarrow 4' \equiv 4 \rightarrow (643\tilde{1})$  and  $6 \rightarrow 6' \equiv (4\tilde{2}\tilde{3}\tilde{1})$ . We finally need to account for the symmetries that must be preserved under inflation. In particular the following identities must hold at every order:

$$1 = \mathcal{T}P_y(4), \quad \tilde{3} = \mathcal{T}R(4), \quad \tilde{2} = R^{-1}P_y(4), \quad \tilde{1} = \mathcal{T}R^{-1}(4), \quad 3 = \mathcal{T}P_x(4). \quad (2)$$

Taking all the above into account, we can write the inflation in terms of the two words  $Q_4$  and  $Q_6$ . If their forms at the k-th approximant are  $Q_4^{(k)}$  and  $Q_6^{(k)}$ , they iterate as follows:

$$\begin{aligned} Q_6^{(k)} &= Q_4^{(k-1)}(R^{-1}P_yQ_4^{(k-1)})(\mathcal{T}RQ_4^{(k-1)})(\mathcal{T}P_yQ_4^{(k-1)}) \\ Q_4^{(k+1)} &= Q_6^{(k)}Q_4^{(k)}(\mathcal{T}P_xQ_4^{(k)})(\mathcal{T}R^{-1}Q_4^{(k)}). \end{aligned} \quad (3)$$

We remind that the word  $Q_4^{(k)}$  determines only the lower left quarter of the full pattern  $W^{(k)}$ . The explicit form of the latter is obtained by using the symmetries:

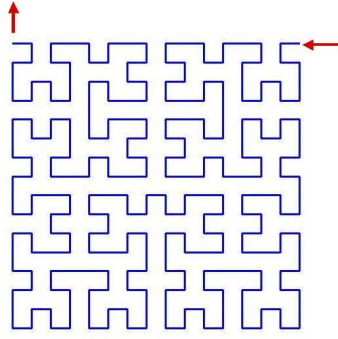


**Figure 2.** Closed  $PH_2$  chain, also known as Moore curve: we display here the lower left quarter ( $L\mathcal{L}$ ) of the approximant of order  $k=4$ ; the arrows depict the ingoing and outgoing links connecting this quarter to its neighbours. One can notice that the connection to the neighbour lying on the right side is provided by an horizontal link placed at the uppermost available location. A complementary situation regards the connection with the upper neighbour: in this case the link is vertical and is placed at the leftmost available location. The inflation procedure is defined in such a way as to guarantee that this structure is preserved at all orders.

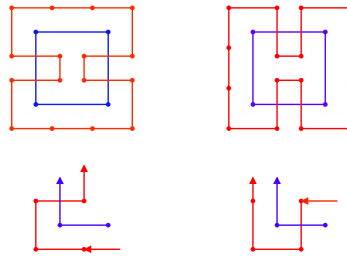


**Figure 3.** In the lower line of this figure are displayed the two choices available when inflating the vertex  $m = 4$ ; the parent (inflated) patterns are depicted in blue (red). With the left choice, the new vertices formed at the entrance and at the exit of the  $m = 4$  motif are respectively a flat horizontal ( $\tilde{5}$ ) and an orthogonal ( $\tilde{3}$ ). The convention chosed in the paper is displayed on the right: an horizontal link enters the orthogonal vertex ( $\tilde{1}$ ), and a vertical link exits the flat vertical vertex 6. In the upper part of the figure we display the two resulting closed patterns after one step of the inflation procedure; the initial configuration is the squared perimeter depicted in blue. The two complementary H-shaped portions of the plane enclosed by the red patterns, when glued together as the two patches of a tennis ball, form a compact surface  $S^2$ : hence the approximants separate the compactified plane in two polar regions. The Peano chain is the maximally extended 'equator' of this partition process.

$$W^{(k)} = Q_4^{(k)}(\mathcal{T}P_x Q_4^{(k)})(P_x P_y Q_4^{(k)})(\mathcal{T}P_y Q_4^{(k)}).$$

### 3. Elastic network and trace map

The two-component vector field of planar elastic deformations, when assigned in lattice coordinates has the form  $\vec{X}(i, j) \equiv (x(i, j), y(i, j))$ . Here we consider a  $(2^k \times 2^k)$  lattice; the indices  $(i, j)$ ,  $(i, j = 1, 2, \dots, 2^k)$  correspond to the  $(x, y)$  coordinates. From the lattice representation we go over to the Peano coordinates:

$$\vec{X}(i, j) \equiv (\vec{x}(1), \dots, \vec{x}(n), \dots, \vec{x}(4^k)). \quad (4)$$

In the model it is assumed that the elasticity is transmitted only along the D=1 path determined by the Peano pattern, hence the elastic energy depends on the ordered sequence of links and vertices as assigned by the chain. If one disregards the fluctuations, the time evolution equation has the following local form:

$$\left(\frac{d}{dt}\hat{\mathbf{I}} - \hat{V}_n\right)\vec{x}(n) = \hat{\Gamma}_n^{(in)}\vec{x}(n-1) + \hat{\Gamma}_n^{(out)}\vec{x}(n+1) \quad (5)$$

As one can see it is of second order in the chain coordinate  $n$  and has a  $(2 \times 2)$  matrix form, since it couples the two-dimensional spaces of elastic deformations attached to the chain sites  $(n-1, n, n+1)$ ; furthermore, we have chosen an orientation for the path. The  $(2 \times 2)$  matrices  $\hat{V}$ ,  $\hat{\Gamma}^{(in)}$ ,  $\hat{\Gamma}^{(out)}$  describe on-site and hopping contributions, with obvious notation. We consider here an anisotropic elastic network: when the deviations are orthogonal to the link's alignment they pay an energy higher than when they are parallel to it. We label with a  $t$  (transverse) and with an  $l$  (longitudinal) the corresponding elastic constants:  $k_t, k_l$ , ( $k_t > k_l$ ). In the polymeric interpretation of the model it is appropriate to consider in addition a coupling  $\gamma$  associated with the angular bending at the vertices. We point out that due to the anisotropy even in the absence of this angular contribution the model has no soft (zero energy) modes, apart from uniform translation. The following condition, which is enforced throughout the paper:

$$\hat{V}_n + \hat{\Gamma}_n^{(in)} + \hat{\Gamma}_n^{(out)} = \hat{0}, \quad (6)$$

guarantees that the spectrum has its bound at  $\Lambda = 0$ . As long as the contact interactions among non-subsequent sites are not taken into account, the elastic modes are sustained only along the chain's pattern. We will discuss in the next Section the relaxation of the vector field  $\vec{X}(t)$  described by the linear Langevin equation:

$$\frac{d}{dt}\vec{X}(t) = \mathcal{D} \cdot \Delta_{(PH)}\vec{X}(t) + \vec{\xi}(t) \quad (7)$$

$$\langle \xi_i(n, t)\xi_j(n', t') \rangle = 2 \cdot \mathcal{D} \cdot k_B T \cdot \delta_{i,j} \cdot \delta(t-t') \cdot \delta_{n,n'}, \quad (i, j = x, y).$$

This process can be considered an inhomogeneous generalization of the well-known Rouse model, where the chain laplacian  $\Delta_{(PH)}$  is disordered. The critical dynamics of Rouse chains and membranes has been studied by K.J.Wiese [25]; in that work the self-avoidance was taken in full account. Here we are studying a purely linear system,

but with a nontrivial dependence on the geometry of the underlying pattern. In this Section we formulate the spectral problem for the noiseless equation, obtained from the above by letting  $(d/dt \rightarrow \lambda, T = 0)$ . As previously noticed,  $\Delta_{(PH)}$  is not a scalar operator: it couples the vector spaces of deviations  $(x, y)$  attached to the chain sites  $(n+1, n, n-1)$ . When the bending contribution is disregarded ( $\gamma = 0$ ),  $\Delta_{(PH)}$  becomes diagonal in the x and y components:

$$\Delta_{(PH)} \equiv \text{Diag}(\Delta_x(k_t, k_l), \Delta_y(k_t, k_l)). \quad (8)$$

One thus has two scalar disordered laplacians: the two are equivalent since they turn one into the other upon exchanging the coupling constants:  $k_t \rightarrow k_l, k_l \rightarrow k_t$ , we have:

$$\Delta_y(k_t, k_l) = \Delta_x(k_l, k_t). \quad (9)$$

From now on we will study  $\Delta_x$ . The equation for the component  $x(n, t)$  involves the outgoing  $(n+1, n)$  and ingoing  $(n, n-1)$  links:

$$\begin{aligned} (\lambda - V_n)x(n) &= \Gamma_n^{(in)}x(n-1) + \Gamma_n^{(out)}x(n+1) \\ (\Gamma_n^{(out)} &= \Gamma_{n+1}^{(in)}) \end{aligned} \quad (10)$$

Here the hopping coefficients  $\Gamma$  have value  $k_l(k_t)$  at the horizontal (vertical) links. The site (vertex) potential  $V$  is given by  $V_n = -(\Gamma_n^{(in)} + \Gamma_n^{(out)})$ ; as announced, in this way the uniform solution, which describes the Peano chain, corresponds to  $\lambda = 0$ . By following a standard procedure the local equation is written in the form of a single step map over a two-dimensional space: from  $\vec{z}(n) \equiv (x(n), x(n-1))^T$  to  $\vec{z}(n+1)$ :  $\vec{z}(n+1) = T(n)\vec{z}(n)$ . We introduced the transfer matrix  $T \equiv T(n)$ , which is assigned to the vertex where the two links involved meet together:

$$\begin{aligned} T(n)_{1,1} &= \frac{(\lambda - V_n)}{\Gamma_n^{(out)}}, \quad T(n)_{1,2} = -\frac{\Gamma_n^{(in)}}{\Gamma_n^{(out)}} \\ T(n)_{2,1} &= 1, \quad T(n)_{2,2} = 0 \end{aligned} \quad (11)$$

The eigenvalue problem for the disordered laplacian  $\Delta_x$  is finally formulated as a boundedness condition for the transfer matrix of the total chain  $T_{tot} \equiv T(N_k) \cdot T(N_k - 1) \cdot \dots \cdot T(2) \cdot T(1)$ . One requires that  $T_{tot}$  must be bounded; If one were to operate with  $SL(2, R)$  matrices (i.e. determinant +1 matrices) the boundedness condition for  $T_{tot}$  would be limited to a single condition on the trace:  $\frac{1}{2}|\text{Trace}(T_{tot})| \leq 1$ .

It is thus convenient to formulate the problem in terms of  $SL(2, R)$  matrices. This can be readily done by performing the following transformation:

$$T(n) \rightarrow \hat{T}(n) \equiv S^{-1}(n+1) \cdot T(n) \cdot S(n), \quad S(n) = \mathbf{1}/(\Gamma_n^{(in)})^{1/2}$$

The new matrices  $\hat{T} \equiv \hat{T}_{out,in} = \hat{T}(\alpha, \beta)$  belong to  $SL(2, R)$ ; they have the form:

$$\begin{aligned} \hat{T}_{1,1} &= \frac{\lambda}{\beta} + \alpha + \frac{1}{\alpha}, \quad \hat{T}_{1,2} = -\alpha \\ \hat{T}_{2,1} &= 1/\alpha, \quad \hat{T}_{2,2} = 0 \end{aligned} \quad (12)$$

The parameters  $\alpha, \beta$  are functions of the hopping coefficients:  $\alpha \equiv \alpha(n) = (\frac{\Gamma_n^{(in)}}{\Gamma_n^{(out)}})^{1/2}$  and  $\beta \equiv \beta(n) = (\Gamma_n^{(out)} \cdot \Gamma_n^{(in)})^{1/2}$ . It seems then that the inflation rule for symbolic words can be formulated in terms of transfer matrices. There is a difficulty here: we must still determine how the inversion operator  $\mathcal{T}$ , which appears explicitly in the inflation, is represented in the present context. One can notice that  $\mathcal{T}$  has the effect of exchanging  $\Gamma^{(out)}$  with  $\Gamma^{(in)}$ ; in fact it must be :  $\mathcal{T}(\hat{T}_{out,in}) = \hat{T}_{in,out}$ . In this way we represent the action of  $\mathcal{T}$  as follows:

$$\mathcal{T}(\hat{T}(\alpha, \beta)) = \hat{T}(1/\alpha, \beta) = \sigma_1 \cdot \hat{T}^{-1}(\alpha, \beta) \cdot \sigma_1. \quad (13)$$

Here  $\sigma_1$  is the Pauli matrix [ $(\sigma_1)_{12} = (\sigma_1)_{21} = 1, (\sigma_1)_{11} = (\sigma_1)_{22} = 0$ ]. We can now proceed to obtain the inflation equations for the transfer matrices. In order to construct the chain's pattern the single-step transfer matrix  $\hat{T}_{out,in}$  must occur in four different forms:  $\hat{T}_{xy}, \hat{T}_{xx}, \hat{T}_{yx}, \hat{T}_{yy}$ . Each matrix is attached to a vertex, labeled according with the directions of its outgoing and ingoing links. We finally obtain the inflation rule. Its form for the matrices  $\hat{T}_{yx}$  and  $\hat{T}_{yy}$  is given by:

$$\begin{aligned} \hat{T}'_{yx} &= \hat{T}_{yy} \cdot \hat{T}_{yx} \cdot \mathcal{T}(\hat{T}_{xy} \cdot \hat{T}_{yx}) \\ \hat{T}'_{yy} &= \hat{T}_{yx} \cdot \hat{T}_{xy} \cdot \mathcal{T}(\hat{T}_{yx} \cdot \hat{T}_{xy}). \end{aligned} \quad (14)$$

The formula for the 'conjugate' vertices  $\hat{T}_{xy}$  and  $\hat{T}_{xx}$  is identical, but with exchanged  $x, y$  labels.

If one disregards the action of the inversion operator, one finds here a free group with four generators  $X(1), X(\bar{1}), X(2), X(\bar{2})$ :

$$X(1) \equiv \hat{T}_{yx}, X(\bar{1}) \equiv \hat{T}_{xy}, \quad X(2) \equiv \hat{T}_{yy}, X(\bar{2}) \equiv \hat{T}_{xx} \quad (15)$$

In Fig.4, as an example, we show the linear pattern generated in the plane by alternating the two types of orthogonal vertices  $X(1)$  and  $X(\bar{1})$ . The inversion operator  $\mathcal{T}$  acts on an element  $M \in SL(2, R)$  in the following way:  $\mathcal{T}(M) = \sigma_1 \cdot (M)^{-1} \cdot \sigma_1$ . Hence if we make this  $\sigma_1$ -dependence explicit we obtain:

$$\begin{aligned} \hat{T}'_{xy} &= \hat{T}_{yy} \cdot \hat{T}_{yx} \cdot \sigma_1 \cdot \hat{T}_{yx}^{-1} \cdot \hat{T}_{xy}^{-1} \cdot \sigma_1 \\ \hat{T}'_{yy} &= \hat{T}_{yx} \cdot \hat{T}_{xy} \cdot \sigma_1 \cdot \hat{T}_{xy}^{-1} \cdot \hat{T}_{yx}^{-1} \cdot \sigma_1. \end{aligned} \quad (16)$$

This equation allows to compute the band spectra of periodic approximants of increasingly high order  $k$ . One sweeps the spectral parameter  $\lambda$  in the initial conditions, and then iterates the map up to the order  $k$ . Since the chain pattern is invariant with respect to space reflexions, it is sufficient to require that the solutions are bounded over a quarter of the chain. Rather than proceeding by direct diagonalization of matrix products having an exponentially large numbers of factors, we preferred to study the problem in the space of the traces: this approach allows for a much higher precision. The boundedness condition quoted above translates into:

$$\frac{1}{2} \cdot |\text{Trace}(\hat{T}_{yx} \cdot \hat{T}_{xy})| \leq +1, \quad \frac{1}{2} \cdot |\text{Trace}(\hat{T}_{yx})| \leq +1. \quad (17)$$

The trace map is defined over the variables

$$x(\alpha, \beta, \dots) \equiv \text{Trace}(X(\alpha, \beta, \dots)), \quad (18)$$

$$y(\alpha, \beta, \dots) \equiv \text{Trace}(X(\alpha, \beta, \dots) \cdot \sigma_1),$$

where  $X(\alpha, \beta, \dots) \equiv X(\alpha) \cdot X(\beta) \cdot \dots$ . The labels  $\alpha, \beta, \dots$  run over the four values  $1, \bar{1}, 2, \bar{2}$ . The relevant point to be stressed here is that the space of the traces turns out to be finite-dimensional. This property is a direct consequence of the Cayley-Hamilton (CH) relation

$$M^2 - \text{Trace}(M) \cdot M + \det(M)\mathbf{1} = 0. \quad (19)$$

One can in fact verify that (CH) allows to reduce the order of positive powers of matrices  $M^k$ , ( $k = 2, 3, \dots$ ), and to turn negative powers  $M^{-1}$  into positive ones. More importantly one can show that the traceless parts of the matrices

$$\mathcal{M} \equiv M - \frac{1}{2} \cdot \text{Trace}(M) \cdot \mathbf{1} \quad (20)$$

satisfy Clifford anticommutation rules. An easy way to ascertain this point is to start by writing the matrices in the real representation

$$M = m_0 \cdot \tau_0 + \vec{m} \cdot \vec{\tau}, \quad \text{where } \tau_0 = \mathbf{1}, \quad \tau_1 = i \cdot \sigma_2, \tau_2 = \sigma_3, \tau_3 = \sigma_1; \quad (21)$$

the matrix is thus mapped into a four-dimensional space with coefficients

$$m_0 \equiv \frac{1}{2} \text{Trace}(M), \quad m_i, (i = 1, 2, 3). \quad (22)$$

The algebra of the spin operators  $\tau_i$ , ( $i = 1, 2, 3$ ) allows to compute, for any couple  $A, B$ , the anticommutator  $[A, B]_+$ . In terms of the traceless parts  $\mathcal{A}$  and  $\mathcal{B}$  one finally gets:

$$\mathcal{A} \cdot \mathcal{B} + \mathcal{B} \cdot \mathcal{A} = (A; B) \cdot \mathbf{1}, \quad (23)$$

where  $(A; B) \equiv \text{Trace}(A \cdot B) - \frac{1}{2} \cdot \text{Trace}(A) \cdot \text{Trace}(B)$ .

These rules allow one to collect equal factors within products, so that their powers can be reduced to order one. In this way one gets monomials made up of the four elements  $X(\alpha)$  raised at the most to power one. The occurrence of their time-inverted copies introduces in the algebra the matrix  $\sigma_1$ : one is thus led to operate in the larger space  $SL^\pm(2, R)$ . In practice we work on polynomials with coefficients of the form  $a + b \cdot \sigma_1$  where  $a, b$  are real-valued.

#### 4. Multifractal spectrum

We will now illustrate the numerical results obtained in the simple situation where the  $x$  and  $y$  components of the elastic displacements are decoupled. In our numerical work we started by verifying that in the periodic case  $k_t = k_l$  the map does indeed reproduce the analytical solution. We initialized the iteration procedure by choosing identical

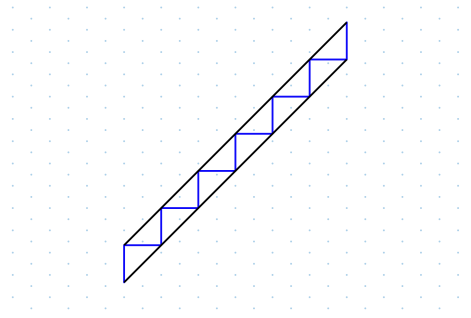


**Figure 4.** Planar strip generated by alternating the two types of orthogonal vertices ( $X(1)$ ,  $X(\bar{1})$ ): the horizontal (vertical) steps of the ladder are associated with discrete translations along  $q_x$ , ( $q_y$ ). The ladder can represent a trajectory undergoing a sequence of scatterings at the strip's boundaries: the corresponding motion, aligned with the strip's direction depicted in black, would carry a linear momentum  $p$  in that direction. This pictorial illustration suggests that the orthogonal vertices, which determine the turning points of the chain, should be associated with translations in the plane  $(p_x, p_y)$  where the axes form an angle  $\pi/4$  with respect to the orientation of the plane  $(q_x, q_y)$ . See also the caption of Fig.8

single vertex transfer matrices  $\hat{T}_0 \equiv \hat{T}(\alpha = 1, \beta)$  and found that the iteration correctly generates the powers  $\hat{T}_0^{N_k}$ ,  $N_k = 4^k$ . More precisely one obtains the traces

$$\text{Trace}(\hat{T}_0^{N_k}) = 2 \cdot \cos(N_k \cdot \theta), \quad \cos(\theta) = \frac{1}{2} \cdot \left( \frac{\lambda}{\beta} + 2 \right), \quad \text{Trace}(\hat{T}_0^{N_k} \sigma_1) = 0. \quad (24)$$

The results reported here refer to a very small anisotropy:  $\gamma = 0$ ,  $k_l = 1 - \epsilon$ ,  $k_t = \frac{1}{k_l}$ , ( $|\epsilon| \ll 1$ ). If one considers e.g. the x-component of the displacement field, with  $\epsilon > 0$  it undergoes a weaker restoring force at the horizontal links than at the vertical ones, i.e. its longitudinal displacements are slightly softer than the transversal ones.

After one iteration the initial band  $-2 \cdot (\alpha + 1/\alpha) \leq \lambda < 0$  splits into four bands, and this branching process repeats itself at the successive steps so that the number of bands  $\mathcal{N}_k$  scales as the size of the system  $\mathcal{N}_k \approx 4^k$ .

This behavior is found provided that  $\epsilon$  is sufficiently small; we found that upon increasing the anisotropy the bands can overlap. In the results displayed here we made sure that the behavior  $\mathcal{N}_k \approx 4^k$  was preserved up to  $k = 10$  iterations.

The spectra of 'disordered laplacians', when characterized in terms of the density of states (DOS)  $\rho(\lambda)$ , can display a variety of scaling behaviors  $\rho(|\lambda|) \approx (|\lambda|)^{\alpha-1}$ ; in general the exponents  $\alpha$  are connected with the dimension of the background lattice where the laplacian is defined as well as with the statistical properties of the disorder.

We remind here that in the literature on phononic spectra it is more common to consider, rather than  $\alpha$ , the spectral dimension  $d_s$  [26] which gives the scaling of the density of states with respect to the frequencies  $\rho(\omega) \approx (\omega)^{d_s-1}$ ; since  $\lambda \equiv -\omega^2$  the two exponents are trivially related  $\alpha = \frac{d_s}{2}$ . Quite surprisingly we have found, close to the isotropic limit, a whole set of power law singularities, over an interval overlapping the value  $\mu = 1$ . As shown in Fig.5 the spectrum is strongly sensitive to disorder even at rather small values of  $\epsilon$ . We did not systematically explore the isotropic limit  $\epsilon \rightarrow 0$  but the

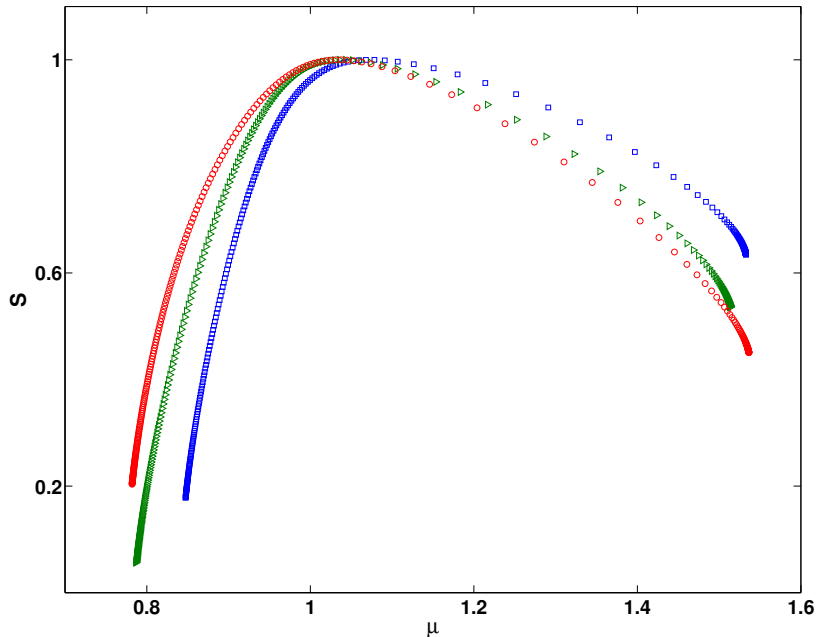


**Figure 5.** Isotropic limit of the disordered laplacian. We display here the distribution  $S(\mu)$  of the scaling exponents  $\mu$  obtained from the periodic approximant of order  $k=10$ . The three plots correspond to increasingly small values of the anisotropy parameter ( $\epsilon = 10^{-5}$  red (circles),  $10^{-6}$  green (triangles),  $10^{-7}$  blue (squares)). It appears that the isotropic limit is characterized by a spectrum which turns out to be qualitatively different from what one would expect in the case of periodic chains (see text). We consider here the distribution for the the exponent  $\mu$ , which defines the scaling of the bandwidths ( $\Delta\lambda \approx \mathcal{N}^{-\mu}$ ). We recall that the more frequently used exponent  $\alpha$  refers instead to the scaling of the density of states (DOS)  $\rho(\lambda) \approx \lambda^{\alpha-1}$ . The two representations are equivalent: in fact from the boundedness of the integrated DOS  $H(\lambda) : \Delta H(\lambda) \equiv \rho(\lambda) \cdot \Delta\lambda = O(1)$  one obtains  $\mu = \frac{1}{\alpha}$ .

whole set of singularities [27] found here is qualitatively different from what one would expect in periodic chains. As it is well known the DOS of periodic chains has only two exponents:  $\mu_{min} = 1$  and  $\mu_{max} = 2$ , where the latter reveals the D=1 Van Hove singularity at the band-edges; its relative weight, with respect to the eigenvalues inside the bands, is irrelevant. In fact  $S(\mu = 2) = 0$ , while  $S(\mu = 1) = 1$ . Here the situation is completely different: we find the continuum spectrum contribution  $\mu = 1$ , hence there are genuine normal modes, herefrom to be called Peano modes, that we will analyze in the next Sessions. In addition we find power-law singularities both below and above  $\mu = 1$ , present with a weight comparable with the Peano modes. It would be rather difficult and computer-time consuming to classify the solutions by means of a systematic analysis of the eigenfunctions. We have found a way out of this problem by studying the correlation functions of the associated relaxation process: the results will be presented in the next Section.

Going back to the spectral analysis, in the case of discretized, disordered extensions of

laplacians, such as the one examined here, typically even within a small spectral range  $\Delta\lambda$  one can find a variety of singularities, so that numerical plots of the DOS versus  $\lambda$  are generally hard to be interpreted. This difficulty, as it is well known, can be surmounted when the singularities are of power-law type; a smooth distribution can be obtained by collecting together the portions of the spectrum which share the scaling exponent. Notice that the localized states, which contribute with delta-like singularities, cannot be detected within this approach. The procedure goes under the name of thermodynamic formalism [28] for multifractals.

One defines a partition function  $Z(\tau)$ , where  $\tau$  is the analog of an inverse temperature; the sum in the present case is taken over the  $\mathcal{N}$  bands of a periodic approximant, and accounts for their individual widths  $\Delta\lambda_l$ , ( $l = 1, \dots, \mathcal{N}$ ):

$$Z(\tau) \equiv \sum_{l=1}^{\mathcal{N}} (\Delta\lambda_l)^{-\tau} \approx (\mathcal{N})^{q(\tau)}. \quad (25)$$

The scaling behaviors are weighted in dependence on the value of  $\tau$ . The exponent  $q(\tau)$  is the analog of a free energy: in fact it is the sum of an entropy and an energy contribution. To see this, consider the subset of bands  $E(\mu)$  whose widths scale as  $\Delta\lambda \approx \mathcal{N}^{-\mu}$ ; if we make the dependence on  $\mu$  explicit on the r.h.s. of the equation, we get:

$$q(\tau) = S(\mu) + \mu \cdot \tau, \quad (\mu \equiv \frac{dq}{d\tau}). \quad (26)$$

The 'entropy' function  $S(\mu)$  is displayed in Fig.4; it weights the different  $\mu$ -scalings within the spectrum, so that its value corresponds to the fractal dimension of the subset  $E(\mu)$ . The extremal values  $\mu_{max,min} \equiv \lim_{\tau \rightarrow \pm\infty} \frac{dq}{d\tau}$  of the support of  $S(\mu)$  characterize the 'vacuum' (temperature  $T \rightarrow 0_+$ ) and the 'fully inverted state' (temperature  $T \rightarrow 0_-$ ) regimes. Notice that from the formula relating  $q(\tau)$  with  $S(\mu)$  one identifies the internal energy  $U$  of the system:

$$U \equiv -\frac{dq}{d\tau} \quad (27)$$

The results displayed in Fig.5 refer to the scalar disordered laplacian  $\Delta_x$ ; this single-component problem describes a 'polarized' D=1 diffusion, as if a blind walker experienced a sequence of varying mobilities encoding the path in its meandering along the plane. The spectrum of the full vector-valued problem is shown in Fig.6: we add here a comment on this case. When the operator  $\Delta_{(PH)}$  is diagonal in  $x$  and  $y$  its eigenstates are obtained from linear combinations of vectors formed using the  $x$  and  $y$  solutions of the single-variable problem:

$$\vec{\alpha}_\lambda(n) \equiv (x_{\lambda_x}(n), 0)^\top \quad \vec{\beta}_\lambda(n) \equiv (0, y_{\lambda_y}(n))^\top \quad (28)$$

The eigenvectors which correspond to the eigenvalue  $\lambda$  of the two-dimensional problem must satisfy the following condition:

$$\lambda = \lambda_y(k_t, k_l) = \lambda_x(k_l, k_t), \quad (29)$$

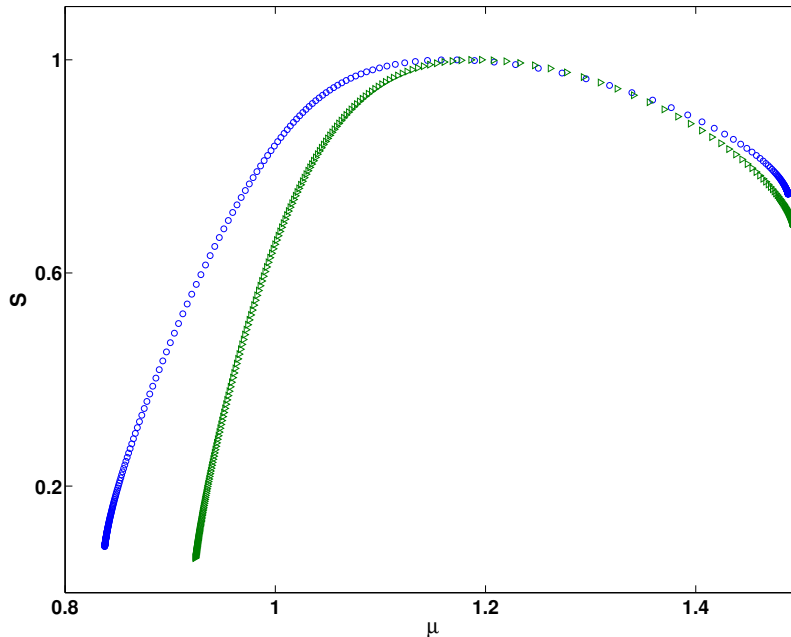


**Figure 6.** Spectrum corresponding to the vector-valued eigenstates: plot of the distribution  $S(\mu)$  obtained with inhomogeneity parameter  $\epsilon = 10^{-4}$ : green (triangles). For comparison we plot the distribution associated with the corresponding single variable problem (blue, circles). The interval  $(\mu_{min}, \mu_{max})$  appears to be contracted in the two-dimensional problem. Thus the requirement that the eigenvalues are at the intersection of the two single-variable spectra  $\lambda_x(k_x, k_y)$  and  $\lambda_y(k_y, k_x)$ , modifies the scaling in the extremal regions  $\mu \approx \mu_{min}$ ,  $\mu \approx \mu_{max}$ .

where  $\lambda_x$  and  $\lambda_y$  are the eigenvalues of the one-dimensional problems. As a consequence, since the spectrum of the vector problem is at the intersection of the two spectra, the support of the function  $S(\mu)$  is smaller than its scalar analog (see Fig.6)

## 5. Langevin equation

We proceed now to examine the relaxation process described by the Langevin equation. Our aim is to characterize the fluctuations by means of the exponents  $\mu$ . For the sake of simplicity we omit the vector indexes and put  $D = 1$  and  $k_B T = 1$ . Our discussion relies on the literature dedicated to dispersion relations of fractals [29] as applied e.g. to the Generalized Gaussian Structures [30]. The relaxation process defined by the Langevin equation is fully described by the response function (also called dynamic susceptibility) and by the correlation function; these two functions are related through the fluctuation-dissipation theorem [31]. Before considering our case we remind known facts regarding the gaussian process defined as the relaxation of a field  $\phi(x, t)$  in the presence of white

noise  $\xi(x, t)$ :

$$\frac{d}{dt}\phi(x, t) = -[r - \nabla^2]\phi(x, t) + \xi(x, t). \quad (30)$$

In the energy-momentum representation the dynamic susceptibility of this process is  $\chi(\lambda, \mathcal{Q}) = (-i \cdot \lambda + r + \mathcal{Q}^2)^{-1}$ . The correlation function, defined as  $C_\mu(x, t) \equiv \langle \phi(x, t) \cdot \phi(0, 0) \rangle = \int \frac{d\mathcal{Q}}{2\pi} \int \frac{d\lambda}{2\pi} C(\lambda, \mathcal{Q}) e^{i(\mathcal{Q} \cdot x - \lambda \cdot t)}$  in the energy-momentum representation has the form:

$$C(\lambda, \mathcal{Q}) = 2 \cdot (\lambda^2 + (r + \mathcal{Q}^2)^2)^{-1}. \quad (31)$$

We now relate the diffusive dispersion of the process with the singularity in the spectrum, which here occurs at the band edges: this can be done in the scale-free regime  $r = 0$ . We are going to show that the  $\mathcal{Q}^2$  dispersion is the counterpart of the multiplicity of states at the edges of the spectral region. In order to make this point clear it is convenient to go over to the discretized version of the laplacian, where the counting of the states at the boundary of the spectrum becomes elementary:

$$\frac{t}{2}(\psi_{n+1} + \psi_{n-1} - 2 \cdot \psi_n) = E\psi_n, \quad (\psi(N) = \psi(0)) \quad (32)$$

Consider now the map  $E \mapsto n$  associated with the set of eigenvalues  $E = E(n) \equiv E(k_n) = t(\cos(k_n) - 1)$ , ( $k_n = \frac{2\pi n}{N}$ ): this map is everywhere invertible with the exclusion of the band edges  $E = 0$  and  $E = -2t$ : there the DOS displays the D=1 van Hove singularities

$$d\rho(E') = \frac{1}{2\pi} \frac{dE'}{(t^2 - E'^2)^{\frac{1}{2}}}, \quad (E' \equiv E + t). \quad (33)$$

The points  $n(E)$  when projected over the E-axis give, in the internal part of the band, the scaling  $|dE| \propto |dn|$  and, at the bnd edges,  $|dE| \propto |dn|^2$ : notice that since  $|dn| \approx \mathcal{Q}$ , this scaling relation allows us to say that the laplacian's dispersion  $\mathcal{Q}^2$  and the scaling at the edges actually describe the same fact.

We will now generalize this connection to our disordered chain operator, which, as we are going to show, is associated with anomalous gaussian processes. We can no longer rely on functions but only on scaling behaviors: it is thus understood that our arguments are merely heuristic. Let us consider in the first place the edge which corresponds to the scale-free regime, i.e. the spectral region  $\lambda \approx 0$ , and the momenta having the order of the inverse of the chain length  $N$ :  $\mathcal{Q} \propto \frac{1}{N}$ . In analogy with the procedure that has been used for the laplacian, here we associate to the spectral set  $E(\mu)$ , where, we remind, the singularity is  $|\Delta\lambda| \approx \mathcal{N}^{-\mu}$ , a dispersion relation of the form

$$-\lambda(\mathcal{Q}) \equiv \omega^2(\mathcal{Q}) \approx |\mathcal{Q}|^\mu \quad (34)$$

In other words we associate the contribution to the spectrum generated by  $E(\mu)$  with an anomalous gaussian process undergone by a fluctuating field  $\phi_\mu(\lambda, \mathcal{Q})$ . The dynamical susceptibility of the process has the form

$$\chi_\mu(\lambda, \mathcal{Q}) = (-i \cdot \lambda + |\mathcal{Q}|^\mu)^{-1} \quad (35)$$

This corresponds to the correlation function:

$$C_\mu(\lambda, \mathcal{Q}) = \frac{2}{(\lambda^2 + (|\mathcal{Q}|^\mu)^2)} \quad (36)$$

Upon integrating over the energies  $\lambda$  we end up with the following expression of  $C_\mu(x, t)$ :

$$C_\mu(x, t) \equiv \langle \phi_\mu(x, t) \cdot \phi_\mu(0, 0) \rangle \propto \int \frac{d\mathcal{Q}}{2\pi} \frac{1}{|\mathcal{Q}|^\mu} \exp^{i(\mathcal{Q} \cdot x - |\mathcal{Q}|^\mu \cdot t)}. \quad (37)$$

From this formula one extracts the contribution of  $E(\mu)$  to the infrared behavior of the system. The equal-time correlation function gives the spatial behavior of the fluctuations:

$$C_\mu(n, 0) \approx (n)^{\mu-1}, \quad n \gg 1, \quad (n(L) \approx L^2). \quad (38)$$

Here we replaced the space variable  $x$  with the chain's length parameter  $n$ ; with the variable  $L$  we refer to the linear size of the planar region covered by  $n$  subsequent links. Finally, the large time behavior of the chain sites is given by:

$$C(0, t) \approx (t)^{1-\frac{1}{\mu}}, \quad t \gg 1.$$

We have thus shown that in fact the exponent  $\mu$  determines both the space and time behavior of the fluctuations in the infrared regime. This allows us to classify the different types of fluctuations available to the system.

The region  $\mu < 1$  describes fluctuations that decay as a power law in the length  $n$ , the corresponding eigenfunctions presumably have an oscillating behavior where the amplitudes are progressively reduced with distance, as in destructive interference. In addition, when  $\mu < 1$  the fluctuations are short-lived: they decay with time as a power law. In the region  $\mu > 1$  we find the complementary behavior. The fluctuations grow with  $n$ : they can be characterized in terms of the fractal dimension  $D_f = \frac{2}{\mu-1}$ , or, in the polymeric interpretation, by means of the Flory exponent  $\nu = \frac{1}{D_f} = (\mu - 1)/2$ .

One can wonder how spatially growing functions could be acceptable eigenfunctions: in our opinion one has oscillations with amplitudes growing with  $n$ , so that the boundedness condition can be recurrently fulfilled. Since the oscillations are amplified, in this case presumably there is some constructive interference. The complementarity of the two regions  $\mu < 1$  and  $\mu > 1$  extends to the time dependence. In fact when  $\mu > 1$  the chain sites undergo subdiffusion with an exponent  $\gamma_D = 1 - \frac{1}{\mu}$ ; this behavior can equivalently be characterized by the dynamic exponent  $z = 2/\gamma_D$ .

It is worth mentioning that the anomalous gaussian relaxation process described here trivially fulfills the conditions for the validity of the fluctuation-dissipation theorem; as a consequence the well-known deGennes relation  $z = 2 + D_f$ , which follows from that theorem, is fulfilled for all scaling exponents  $\mu$ . We have intentionally excluded here the case  $\mu = 1$ , which marks the separation of the two complementary regions described above. When  $\mu = 1$  one has proper eigenfunctions, i.e. oscillations with stable amplitudes and normal modes: the Peano modes. In order to understand how phononic excitations can be sustained in spite of the scattering processes at the boundaries of the elastic strip one must examine the symmetries of the system: this will be done in Section 7.

## 6. Inverse energy cascade and phase separation

In this Section we give the global picture of the system's relaxation. In order to do that we rely first of all on the scaling behaviors obtained in the previous Section, but we have found that also the thermodynamic formalism of multifractals, that up to now we have used merely for technical reasons, is in fact suitable of physical interpretation and is consistent with the rest of the picture. As previously pointed out in that formalism there is an analog of the internal energy; it is given by  $U = -\frac{dq}{d\tau}(\tau)$ . The region of negative  $\tau$  describes the inverted system (i.e. the regime of negative temperature), and, as one can see in Fig.7, to the higher values of U. The limit  $\tau \rightarrow +\infty$  corresponds to the thermal ground state  $T = 0$  and to the lowest available value of U. On the basis of the numerical checks that we have done up to now, we have found that the region  $\lambda \approx 0$  is dominated by the scaling  $\mu_{max} > 1$ . Although we presently have no direct elements enabling us to associate the  $\mu < 1$  region to particular regions of  $\lambda$ , we point out that where the dilatation dominates one must have higher energies than in shear-dominated regions. It is thus natural to associate the values  $\mu < 1$  with dilatation-dominated fluctuations, characterized by high energies and large momenta, and the values  $\mu > 1$  with shear-dominated excitations, which are more extended and pay a smaller energy cost. Hence the 'internal energy' U could be in fact taken as an effective potential. If one takes this point of view then the plot reported in Fig.7 can be rather simply interpreted in association with the relaxation process: the overdamped system must evolve towards the region dominated by  $\mu_{max}$ , where the fluctuations are long ranged. It is then clear that if the system is prepared on localized states, it is expected to relax towards the shear-dominated  $\mu > 1$  regime. This behavior was in fact observed in two-dimensional colloids [1, 2] and is intriguingly similar to the inverse energy cascade typical of two-dimensional turbulence [3]. So far we have examined the spectral properties in the closeness of the isotropic limit, where the spectral bands are predominantly separated. The following question then comes about: how this scenario is modified when the anisotropy is sufficiently large to make the bands overlap? The answer to this question, as it turns out, can be read by inspecting Fig.7. We have found that the system undergoes a phase transition [32]: the spectral measure  $S(\mu)$  progressively splits into two separate distributions. Possibly the simplest example of a complete phase separation is provided by the D=1 periodic chain: as we recalled previously, in that case there are only two exponents:  $\mu = 1$  and  $\mu = 2$ . Since their weights are  $S(\mu = 1) = 1$ ,  $S(\mu = 2) = 0$ , the periodic chain is located at the extremal point of a line of phase coexistence, where the phase  $\mu = 2$  is at extinction and the system is fully converted into the  $\mu = 1$  phase. An intermediate, coexistence regime, has been found [33] in the spectrum of the Quantum Ising Quasicrystal. That model describes a chain of spins where the Ising couplings are assigned according to the Fibonacci two-letter substitution rule ( $J_0 \rightarrow J_0 \cdot J_1$ ,  $J_1 \rightarrow J_1$ ) [34]. When the two couplings are nearly equal ( $J_0 \approx J_1$ ) the function  $S(\mu)$  has support on  $\mu_{min} < \mu < \mu_{max}$  where  $\mu_{min} = 1$  and  $\mu_{max} = 2$ , so that the spectrum can be interpreted as being at the coalescence of the two mentioned

phases found in the periodic chain. Upon introducing the inhomogeneity by making the two couplings increasingly different ( $J_0 \neq J_1$ ), the two phases were found to progressively separate. This effect turned out to be independent from the magnetic phase transition of the model, but associated only with the disordering of the chain. Since the quantum spin chain can be converted into a Majorana fermionic chain by way of the Jordan-Wigner transformation, there is some element to argue that the phase separation found in the spectrum had to do with the localization of the Majorana fermions induced by making the two couplings  $J_0$  and  $J_1$  different. In general a phase separation can be hardly detected by inspecting  $S(\mu)$ , because the numerics naturally converge to the convex envelope of the two distributions; in fact  $S(\mu)$  is the Legendre transform of the object of relevance in this context, which is the internal energy  $U$  ( $U = -\frac{dq}{d\tau}$ ). From Fig.7, which shows  $\frac{dq}{d\tau}$  when the anisotropy parameter has value  $\epsilon = 10^{-4}$ , one can notice three inflection points:  $A \approx (-4, .1)$ ,  $B \approx (0, 1.1)$ ,  $C \approx (2., 1.3)$ . At the second order critical point one expects a single inflexion point  $B_0$ , approximately located in the closeness of B. Here we are very close to the critical point and, upon increasing  $\epsilon$ , two maxima are expected to emerge within the two regions delimited by  $(A, B)$  and  $(B, C)$ . Such maxima are displaced with respect to  $\tau = 0$  in opposite directions: they respectively identify a phase where the dominant scaling evolves towards  $\mu_{min}$  and a phase where the scaling is closer to  $\mu_{max}$ . It is not difficult to associate the former (on the left-hand side of the plot) with the solid, dominated by the high energy dilatation modes, and the latter, where fluctuations grow both in  $n$  and in  $t$ , with the shear-dominated liquid. We wish to add that the analogies reported above with two-dimensional colloids involve also the spectral properties. In fact if one were to add to the network model the contact couplings among adjacent but nonsubsequent sites, the new network would describe a sort of textured membrane. The resulting phononic spectrum, in addition to the contributions arising from the Peano pattern, would display in the density of states  $\rho(\lambda)$  a contribution  $\rho(\lambda)_{D=2} \approx \lambda$ , arising from the two-dimensional phonons, as in standard D=2 Debye spectra. It is worth mentioning that the quoted experiments on colloids did in fact display an anomalously high density of states at low frequencies [1, 2], superimposed to the D=2 Debye behavior. Let us add now an argument that applies to D-dimensional Peano chains  $PH_D$ , who are characterized by the following scaling property:  $n(L) \approx L^D$ . Since they are always generated by deterministic inflation rules, one can reasonably expect that their self-similarity should be mirrored into nontrivial spectral properties. The spectral problem, if approached along the lines presented in this paper, would involve transfer matrices of dimension  $(2D \times 2D)$ .

We notice that here, where  $D = 2$ , we have been able to reduce the problem in terms of a trace map only in the degenerate case  $\gamma = 0$ . When  $\gamma \neq 0$  this degeneracy is lost, and the transfer matrices must necessarily operate on a four-dimensional vector space. Hence the numerical resolution in determining the spectrum can be seriously compromised even in the case  $D = 2$ .

One can for the time being try to overcome this complexity by means of a mean-field argument, which here means to work with a single  $\mu(D)$  and to disregard the fluctuations

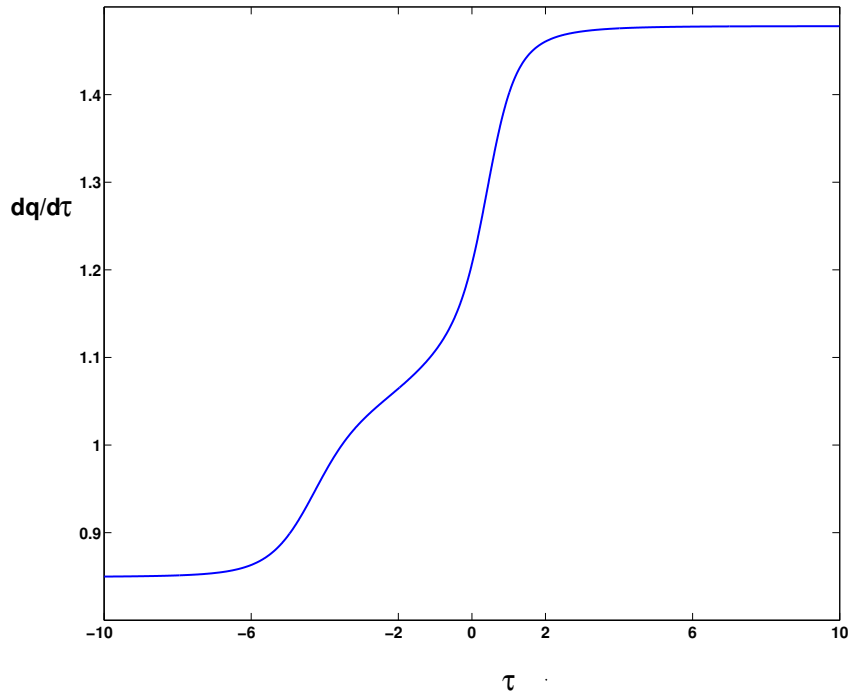


**Figure 7.** Phase separation Plot of the function  $\frac{dq}{d\tau}(\tau)$  obtained from the bands of the approximant of order  $k = 10$ . The inhomogeneity parameter is  $\epsilon = 10^{-4}$ . The 'internal energy'  $U$  of the system is given by  $U = -\frac{dq}{d\tau}$ . The asymptotic values of the function are respectively  $\mu_{min}$ , at large negative values of  $\tau$ , ( $\tau \rightarrow -\infty$ ), and  $\mu_{max}$ , ( $\tau \rightarrow +\infty$ ) at large positive values of  $\tau$ . At the critical (second order) point  $\epsilon \rightarrow 0$  the function  $\frac{dq}{d\tau}(\tau)$  has a single inflexion at  $\tau = 0$ . The plot displayed here clearly shows three inflection points, indicating the onset of the phase separation: the 'internal energy'  $U$  is going to develop two local minima.

of  $\mu$ . Taking into account that the chain is embedded in dimension  $D$ , self-consistency suggests that  $\mu(D)$  should be chosen in such a way as to make the fractal dimension  $D_f$  to coincide with the bulk's dimension:  $D_f = D$ . In order to obtain the function  $\mu(D)$  one can consider a couple of points (1,2) separated by a distance  $r$  in the bulk and then use the general formula relating  $D_f$  with  $\mu$ ; in so doing one finds:

$$\langle (\vec{x}(1) - \vec{x}(2))^2 \rangle \approx r^2 = n^{\frac{2}{D}} = n^{\mu(D)-1}, \quad \mu(D) = 1 + \frac{2}{D}. \quad (39)$$

Notice that in the language of membranes the fluctuating field  $\vec{x}(n, t)$  undergoes the roughening transition at  $\mu = 1$ , hence the mean field exponent corresponds to the membrane being found in the rough phase [35].

In the planar case, which has been studied in this work, one finds the exponent  $\mu(2) = 2 \equiv D_f$ , meaning that the mean field condition is correctly reproduced by the rigid Peano chain. One can notice that the associated elastic network, which accounts for the deformations of the chain, turns out to be less prone to disruption. In fact the maximal growth of the fluctuations in amplitude is determined by  $\mu_{max}$ , and here we have found: ( $\mu_{max} < \mu(2) \equiv 2$ ), ( $\gamma = 0$ ,  $\epsilon \rightarrow 0$ ). In D=3 the exponent is  $\mu(3) = \frac{5}{3}$ ,

wherefrom one derives the anomalous diffusion  $C(0, t) \approx t^{\frac{2}{5}}$ . We point out that it has been found in experiments on bacterial chromosomes [11, 36] that this exponent occurs with high probability. Given the connection established here between time behavior and fractal dimension, the quoted anomalous diffusion exponent is consistent with configurations quite close to the optimal packing  $D_f = 3$  [13]. We conclude this Section with a remark, maybe of utility for some readers: although rather difficult to capture on a purely intuitive basis, fluctuations characterized by a fractal dimension higher than  $D$  cannot be excluded: indeed in some of the measurements quoted above [11] small anomalous diffusion exponents  $\gamma_D < \frac{2}{5}$  were observed, which imply  $1 < \mu < \mu(3)$  and thus  $D_f > 3$ .

## 7. Critical crystal with eightfold symmetry

In the previous Section we have shown that the network model undergoes a phase separation, so that its isotropic limit is found at the saddle separating two phases, respectively of solid and liquid type: the Peano network can be considered a critical crystal, marking the point where coexistence turns into phase coalescence. The situation found here is the  $D=2$  analog of the well studied critical regime at the  $D=1$  delocalization transition, [24, 37]. which can be described within a semiclassical (WKB) approach based on the universal hamiltonian [38]:

$$\frac{1}{2} \cdot H \equiv \cos(p) + \alpha \cdot \cos(q) \quad (40)$$

Exactly at the critical point  $\alpha = 1$  the hamiltonian has a twofold symmetry, since it is self-dual in the exchange of the (adimensional) space and momentum variables. It identifies, in the  $(q, p)$  plane, a square lattice: the lattice points are at the saddles where separatrices meet. The separatrices are soliton trajectories of energy  $H = 0$ ; apart from them, every other orbit is closed, so that when  $\alpha = 1$  the particles are confined both in the  $q$  and in the  $p$  direction.

When self-duality is broken, e.g. when  $\alpha > 1$ , aligned solitons merge into trajectories running parallel to the  $p$ -axis: in this region the particles are localized with respect to the  $q$ -direction. At the complementary value of the coupling ( $\frac{1}{\alpha}$ ) one finds the dual trajectories: the particles are extended in the  $q$ -direction. It resulted from Wilkinson's analysis that the critical properties obtained with the universal hamiltonian, which has a twofold symmetry, actually hold for an entire class of hamiltonians, characterized by fourfold symmetry. An example of such hamiltonians is the following one:

$$\frac{1}{2}H \equiv \cos(q) + \cos(p) + \cos(2 \cdot q - p) + \cos(q + 2 \cdot p) \quad (41)$$

This fourfold symmetry is associated, we believe, with the two generator group  $A, B$ , where  $A, B$  describe discrete translations in the  $q$  and  $p$  directions, when also the time-reversed counterparts are taken into account.

From this perspective the validity of the semiclassical analysis in the closeness of the

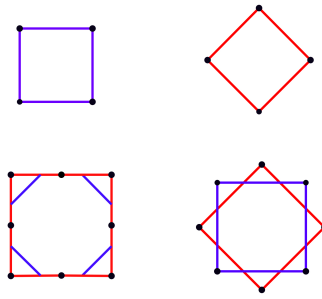


**Figure 8.** Graphical representation of the elementary operations acting on the four-dimensional lattice. Upper line: the blue (red) square path represents the loop of discrete translations in the  $p$ -plane ( $q$ -plane); Lower line, right side: the eightfold motif obtained by projecting the  $p$ -loop on the plane of the  $q$ -loop.

Lower line, left side: the loop formed by combining the eight operators which generate the Peano chain. Here the colour convention is consistent with the rest of the Figure. The red lines represent paths in the  $q$ -plane, the red square is thus associated with a loop in the  $q$ -plane which involves two generators together with their time-inverted copies. The black dots represent the vertices, hence the flat vertices  $X(2)$ ,  $X(\bar{2})$  carry only red lines. We have decorated with blue lines the orthogonal vertices  $X(1)$ ,  $X(\bar{1})$ , which describe the bendings of the chain. The blue segments are aligned with the translations on the  $p$ -lattice, as illustrated previously in Fig.4

delocalization transition is spelled, in the language of trace maps for Fibonacci chains, by the equation  $Trace(A \cdot B \cdot A^{-1} \cdot B^{-1}) = 2$ . In fact this equation marks the change in topology of the invariant surface  $I = x^2 + y^2 + z^2 - x \cdot y \cdot z$ , where two separate classes of dynamics meet [21].

We leave to future work [?] a detailed analysis of the trace map, here we will limit ourselves to show that at the D=2 delocalization transition it is natural to expect an eightfold symmetry. A pictorial view that we hope the Reader will find of some help is presented in Fig.8, where we report the different types of discrete translations which operate on the  $(2 \times 2)$  phase space. The pattern on the lower left is obtained by combining the four vertices  $X(1)$ ,  $X(\bar{1})$ ,  $X(2)$ ,  $X(\bar{2})$  together with their time-reversed copies. The pattern on the lower right is obtained by projecting the  $(p_x, p_y)$  lattice over  $(q_x, q_y)$ . In the usual coplanar representation of the union of a square  $q$ -lattice with its dual, one assigns the nodes of the dual to the centers of the  $q$ -plaquettes; with this convention the tiling appears in the form of two equally oriented square lattices. The eightfold motif obtained here results instead from the convention of making the centers of the  $q$  and  $p$  plaquettes to coincide and to having them rotated of an angle  $\pi/4$ .

This turns out to be the condition which correctly reproduces the geometry associated with the operators  $X(1)$ ,  $X(\bar{1})$ ,  $X(2)$ ,  $X(\bar{2})$ , as shown in the lower line of the figure: one can verify that the two tilings obtained by iterating the two lower figures are identical, when the blue segments are continued up to their intersection. The eightfold symmetry reminds us of the octagonal quasicrystal. It turns out that in recent experiments on bilayer water, precursors of crystallization were observed to generate, together with

quadratic and hexagonal, also pentagonal patterns, but, more importantly, also the dodecagonal quasicrystal [4]. On very general grounds, since quasicrystals are much softer than solids, it is somewhat to be expected that in the liquid to solid transition various structures of intermediate stability should be explored by the system.

As anticipated, in our context the octagonal symmetry has an important role, and one is thus led to consider, as a natural candidate, the octagonal quasicrystal. The question is then: to what extent is the Peano chain related with the octagonal quasicrystal?

The effective coordination number of the Peano network is certainly smaller than the average coordination number of the octagonal quasicrystal. Periodic approximants of the latter [39], obtained by projecting the 4D hypercube on the plane, have square-shaped elementary cells. Each cell has vertices with coordination numbers varying from three to eight ( $z = 3, 4, 5, 6, 7, 8$ ). The free particle quantum motion defined over such tilings is characterized by anomalous diffusion, but with exponents much larger than those obtained here [40].

The reason for that can be easily understood, since in the octagonal quasicrystal there is a larger number of channels open to hopping.

The point we would like to stress here is that the octagonal symmetry arising in the Peano chain does not descend from the euclidean metrics, but from the hamiltonian structure. In fact the partition of the phase space into a  $p$  portion and a  $q$  portion can be wrongly interpreted as orthogonality if quantization is performed in a flat space. Let us then illustrate how the octagonal symmetry emerges here. As one may remind, in order to generate the chain one needs a four generator group. Two of such generators define the discrete translations on the lattice of  $q$  coordinates; in fact the matrices  $X(2)$ ,  $X(\bar{2})$  are associated with the flat vertices, in the two directions available in the plane. The remaining two generators are associated with the orthogonal vertices, which can represent a turn from an horizontal to a vertical link or viceversa: they occur in the two forms  $X(1)$ ,  $X(\bar{1})$ . This does not make the picture complete, since one must in addition consider the time-reversed images of these four generators. In summary, by suitably ordering the resulting eight objects one obtains a loop in the form of an octagon (see Fig.8)

To be specific, in order to quantize an hamiltonian system over a  $(2 \times 2)$  phase space, one needs a  $(4 \times 2)$  generator group, whose elements describe how discrete translations (operating on the  $(q_x, q_y)$ ,  $(p_x, p_y)$  lattice), together with their time-reversed partners, operate on the dynamical variable, which in the present case has values in a real two-dimensional vector space.

If the system is integrable the hamiltonian is quadratic. In the isotropic limit the rotational invariance implies the following form:

$$H = \alpha \cdot (p_x^2 + p_y^2) + \beta \cdot (q_x^2 + q_y^2). \quad (42)$$

At the delocalization transition the system is self-dual, thus at the critical point one has  $\alpha = \beta$ :

$$(p_x^2 + p_y^2) = (q_x^2 + q_y^2) = \frac{1}{2 \cdot \alpha} \cdot H \quad (43)$$

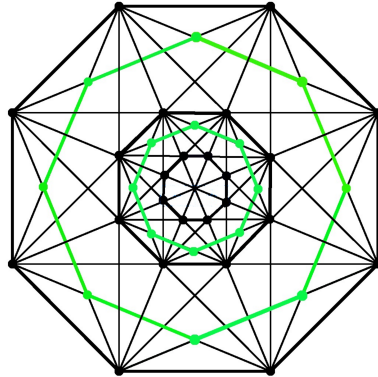


**Figure 9.** The octagon and its descendants: this figure illustrates how the octagonal symmetry is compatible with dilatations. Discrete rotations and discrete dilatations match, as in regular crystals discrete rotations match with lattice translations. This is a sort of polar crystal, not to be confused with the octagonal quasicrystal. Periodic approximants of the octagonal quasicrystal are obtained by projecting the 4D hypercube on the plane: the resulting tilings turn out to have an average connectivity substantially higher than the Peano chain.

In summary, the available solutions are the lattice points lying on an  $S^3$  sphere (embedded in a  $(2 \times 2)$ -dimensional space) which satisfy the above self-duality condition. When the  $\vec{p}$  lattice is projected onto the  $\vec{q}$  plane, the resulting mesh has two intersecting lattices, forming an angle  $\pi/4$  (see Fig.8). As shown in Fig.9 the octagon reproduces itself at various discrete scales. In our context the discrete dilatations match with discrete rotations at the rescalings that correspond to the inflation procedure. An approximant of a given order  $k$  includes the recurrences of the preceding ones. At least this is what one is led to conclude when inspecting the behavior of the density of states versus  $\lambda$ , exhibited in Fig.10. One can notice the following features. A) The distribution undergoes wild fluctuations within small ranges  $\Delta\lambda$ : this was expected, considering the self-similarity of the chain. B) The points frequently fall along several curves; we did not inspect the geometry of these curves, but their shapes are similar to what expected with periodic chains. It is easy to distinguish five curves  $\mathcal{N}(l, \lambda)$ , ( $l = 1, 2, 3, 4, 5$ ). The lengths of the chains grow with the parameter  $l$ : in fact the values of  $\mathcal{N}$  at the intercepts with the vertical axis have equal separation: the number of sites grows as  $4^l$ . C) There is a family of curves  $\sigma$  orthogonal to the previous ones. We colored in red some points that appear to be lying at the intercepts of the  $\mathcal{N}(l, \lambda)$  curves with these  $\sigma$ s. One can give a parametric representation of the  $\sigma$ s in terms of  $\lambda$  and of their arc parameter  $s$ :  $\sigma \equiv \sigma(\lambda, s)$ . E.g. one can use the convention of choosing  $\lambda$  as the intercept of  $\sigma$  with the  $\lambda$  axis:  $\lambda \rightarrow \sigma(\lambda, s = 0)$ . D) As the arc parameter  $s$  sweeps a  $\sigma$  curve corresponding to a fixed parameter  $\lambda$ ,  $\sigma(\lambda, s)$  intercepts approximants of increasingly large order; this

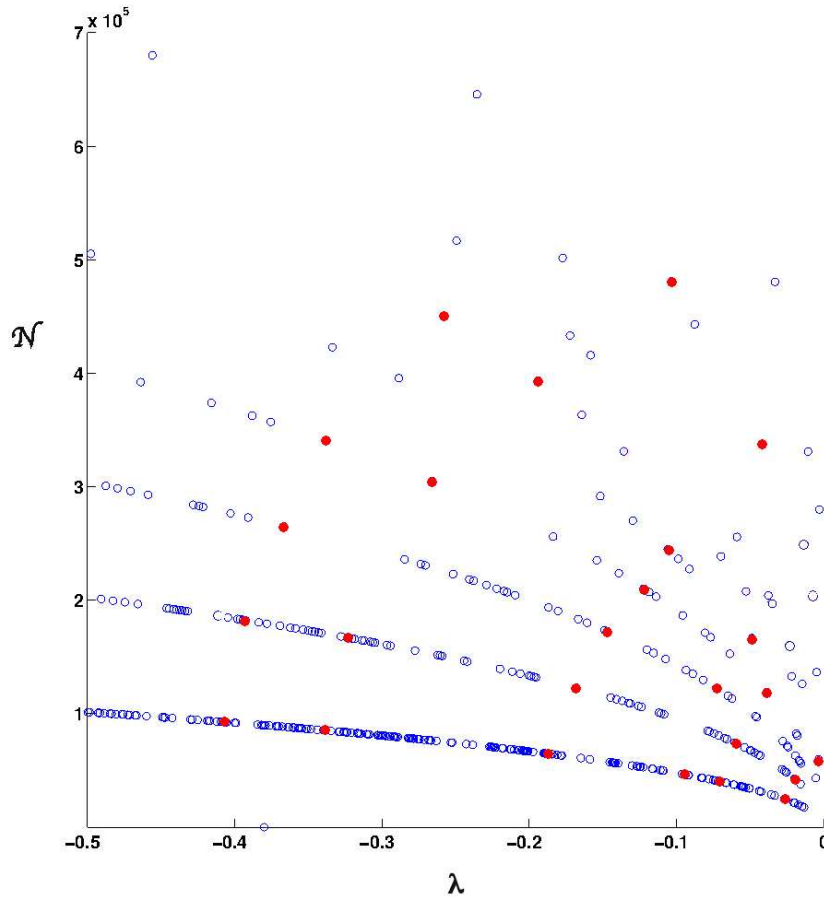


**Figure 10.** Peano modes at the matching conditions of the polar crystal (see Fig.8). Plot of the number of occupied states  $\mathcal{N}$  versus the energy  $\lambda$  in the closeness of  $\lambda = 0$ ; apart from the normalization, it corresponds to the density of states (DOS)  $\rho(\lambda)$ . The data reported here correspond to the approximant of order  $k=6$ , with anisotropy parameter  $\epsilon = 10^{-6}$ , we are thus quite close to the critical point. One can notice that the points of the distribution frequently fall along several curves; the curves have the shape expected with periodic chains. It is easy to distinguish five curves:  $l = 1, 2, 3, 4, 5$ . We colored in red some points of the distribution that appear to be lying at the intercepts of the  $\rho$  curves with a family of curves  $\sigma$  orthogonal to the  $\rho$ s. One can label the red curves with the energy value at their intercept with the horizontal axis:  $\sigma \equiv \sigma(\lambda)$ . As each curve is swept, it intercepts approximants of increasingly large orders

corresponds to degeneracies of increasing order of the eigenvalue  $\lambda$ . We conclude this section with some comments on the symmetries of lower order that can be found in the system when the full isotropy is broken. A quite relevant property of the trace map refers to traces of monomials of order three [?]. These variables represent discretized second order derivatives; they can assume different values, due to the anisotropy of the model. One can classify the cubic monomials on the basis of the trace's invariance under cyclic permutations. This obvious symmetry enforces conditions on the anticommutator

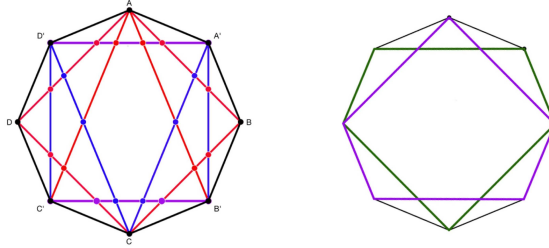


**Figure 11.** Symmetries of lower order compatible with the octagon. One can identify the fourfold loop in the  $q$ -plane (in blue)  $A'B'C'D'$ , and, in red, its analog in the  $p$ -plane  $ABCD$ . Triangular loops mix the  $q$  and  $p$  coordinates; we show here two such loops:  $AB'C'$  and  $CD'A'$ . On the right hand side we display two fivefold loops: they are obtained by connecting the five vertices left out of the triangular loops shown on the left; the fivefold loop depicted in green is the complement of  $AB'C'$ . Within a semiclassical description the loops can be associated with scattering processes adding up to zero momentum exchange, required by the scale invariance at the critical point

algebra, and as a result the traces of cubic monomials can be written in terms of traces of lower order monomials. One thus gets several conservation laws for the map, in particular associated with the order three. In Fig.11 we enumerate some of the various symmetries available.

## 8. Conclusions

We studied the elastic deformations of the plane-filling closed Peano chain; taken as an elastic network, our model has no zero-energy modes.

The bare shear and dilatation modes are intrinsically coupled in the model, because their waves are constrained to propagate along a thin planar strip undergoing the sequence of turns dictated by the deterministic pattern of the chain.

The situation is thus similar to the well known interference, at the surface of a material's bulk, giving rise to the dispersive Rayleigh waves. The Peano chain is characterized by the mentioned deterministic pattern, which has the property of being self-similar, with periodic approximants. In a situation of this type the Rayleigh waves can find resonance conditions necessary for coherent propagation: we have called the corresponding modes Peano modes. They occur when the rescaling associated with the inflation procedure matches with the discrete rotational symmetry of the pattern. We studied the properties of the spectrum by means of the so-called thermodynamic formalism for multifractals. In addition to the Peano modes we have found solutions that can be qualitatively de-

scribed as oscillating functions modulated by amplitudes which grow or decay with a power law behavior. These anomalous modes result from the frustrated coupling of shear and dilatation: when the resonant conditions are not exactly fulfilled, these waves can be amplified or damped, depending on how interference operates. These anomalous behaviors are associated here with gaussian relaxation processes characterized by an anomalous scaling exponent  $\mu \neq 1$ . When  $\mu < 1$  the correlation function decays with respect to the chain coordinate  $n$  as  $n^{\mu-1}$ , hence these states are of localized type. They decay in time as well, with the power law  $t^{1-\frac{1}{\mu}}$ . Although it is rather hard to connect the exponents  $\mu$  to the eigenvalues  $\lambda$ , we have predominantly found the large exponents  $\mu > 1$  in the region  $\lambda \approx 0$ . It is then reasonable to associate to that region these latter states: rather than damping in time, they display anomalous diffusion. Their space dependence is characterized by amplification. Taking the above into account, the relaxation of the system can be described as a flow from localized high energy structures towards extended low energy ones, where the latter survive and actually cumulate in the long time regime of the process. This turns out to reproduce, at least qualitatively, the behavior observed in two-dimensional colloids [1, 2], where initially localized excitations evolve towards large scale structures. It may then be not coincidental that also the presence, observed in the same experiments, of a low-energy bosonic peak, can be readily explained within our model. In our opinion the peak reveals an elastic energy contribution associated with closed, large-sized one-dimensional structures. Structures of this sort are not easily described within a membrane-like network model. The density of states should then account for these excitations, which add up to the standard D=2 phononic part.

Possibly the main result presented in this paper is the existence of a critical point in the isotropic limit of the model, where two phases coalesce. These phases are respectively dominated by the  $\mu < 1$  and  $\mu > 1$  regimes: localized versus delocalized, or, in other words, solid versus liquid. It is thus appropriate to consider the Peano network as a critical crystal, which is definitely softer than a quasicrystal.

As previously illustrated, since the dilatation modes have higher energies and are more localized, during relaxation the energy flows towards extended configurations and lower energies, as in the so-called inverse energy cascade of two-dimensional turbulence. We have found an eightfold symmetry at the critical point: hence the Peano chain turns out to be quite close to the octagonal quasicrystal. Quite intriguingly experiments on bilayer water revealed structures corresponding to the dodecagonal quasicrystal[4]. We point out that the model presented here deals with elastic excitations supported by one-dimensional structures: this makes it solvable but certainly limits its application. From the perspective of the possible connections with the spatial ordering of chromosomes, we previously mentioned that our mean-field estimate of the anomalous diffusion exponent in the D=3 case fits quite well with the numbers observed in bacteria. We finally add a comment regarding other collective excitations to be expected in Peano-shaped structures. The chain phonons treated in this work apply to small deviations with respect to a fully ordered (T=0) Peano chain, but at higher energies one should also isolated

topological defects, that give rise to mismatches in the exact space-filling structure. The motion of defects of this type involves collective reorderings along the chain i.e. phasons [41]. We are led to associate with excitations of this kind the correlated motions observed in chromatin [42]. At even higher energies multiple defects are to be expected, but this goes far beyond the perspective of this paper. We would like to point out that the chain phonons should in any case give a relevant contribution in the infrared limit: in fact their momenta are the smaller available to the system, because they scale as  $L^{-D}$ .

### The Acknowledgements

The Author is indebted to M.Cosentino Lagomarsino for showing him that life may still be found at the boundaries of maximally connected networks, and wishes to thank F.Prati and R.Artuso for reading this zero-mileage product.

### Bibliography

- [1] Z.Zhang D.T.N.Chen P.J.Yunker S.Henkes C.Brito O.Dauchot W. van Saarloos A.J.Liu K.Chen, W.G.Ellenbroek and A.G.Yodh. *Phys.Rev.Lett.* **105**,025501, 2010.
- [2] P.Schall J.Kurchan A.Ghosh, V.K.Chikkadi and D.Bonn. *Phys.Rev.Lett.***105**,02551, 2010.
- [3] P.Tabeling. *Phys.Rep.* **362**,1, 2002.
- [4] N.Kastelowitz J.C.Johnston and V.Molinero. *J.Chem.Phys.***133**, 154516, 2010.
- [5] A.Lempel and J.Ziv. *IEEE Trans.Inf.Theory* **IT-32**,2, 1986.
- [6] N.Merhav A.Cohen and T.Weissmann. *IEEE Trans.Inf.Theory* **35**, 3001, 2007.
- [7] A.Hoorfar J.Zhu and N.Engheta. *IEEE ANTENNAS AND WIRELESS PROPAGATION LETTERS* **3**, 004.
- [8] A.Y. Grosberg, S.K. Nechaev, and E.I. Shakhnovich. *J.Physique(France)* **49**,2095, 1988.
- [9] E. Lieberman-Aiden, N.L. van Berkum, L.Williams, M.Imakaev, T.Ragoczy, A.Telling, I.Amit, B.R.Lajoie, P.J.Sabo, and M.O.Dorschner et al. *Science* **326**,289, 2009.
- [10] M.Dekker J.Dekker, K.Rippe and N.Kleckner. *Science*, **295**,1306, 2002.
- [11] S.C. Weber, A.J. Spakowitz, and J.A. Theriot. *Phys.Rev.Lett.* **104** (23),238102, 2010.
- [12] R.Reyes-Lamothe, C.Possoz, O.Danilova, and D.J.Sherratt. *Cell* **133**,90, 2008.
- [13] V.G. Benza, B.Bassetti, K.D.Dorfman, V.F.Scolari, K.Bromek, P.Cicuta, and M.Cosentino Lagomarsino. *Rep.Prog.Phys.* **75**,076602, 2012.
- [14] C.Zhang and Q.Niu. *Phys.Rev. A* **81**,053803, 2010.
- [15] G.Castaldi V.Galdi A.Alu' N.Engheta A.Silva, F.Monticone. *Science* **343**,160, 2014.
- [16] F.H.Stillingner and Z.W.Salsburg. *Journ.of Stat.Phys.* **1**,179, 1969.
- [17] O.Farago and Y.Kantor. *Phys.Rev.* **E61**,2478, 2000.
- [18] B.Fisher A.Ferguson and B.Chakraborty. *Europhys.Lett.* **66**,277, 2004.
- [19] C.Brito and M.Wyart. *J.Stat.Mech.*, L08003, 2007.
- [20] C.Brito and M.Wyart. *Europhys.Lett.* **76**,149, 2006.
- [21] M. Kohmoto, B. Sutherland, and C. Tang. *Phys.Rev.***B35**,2,1020, 1987.
- [22] J.A.Ashraff, J.M.Luck, and R.B.Stinchcombe. *Phys.Rev. B* **41**,4314, 1990.
- [23] J.M.Luck, C.Godreche, A.Janner, and T.Janssen. *J.of Phys.A:Math.Gen.***26**,1951, 1993.
- [24] S.Aubry and G.Andre'. *Annals of Israel Phys.Soc.* **3**,133, 1980.
- [25] K.J. Wiese. *Eur.Phys.J.* **1**,269, 1998.
- [26] R.Rammal and G.Toulouse. *J.Physique-Lettres* **44**,L13, 1983.
- [27] J.M.Luck and D.Petritis. *J.of Stat.Phys* **42**,289, 1986.
- [28] T.C. Halsey, M.H. Jensen, L.P. Kadanoff, I. Procaccia, and B.J. Shraiman. *Phys.Rev.***A33**,1141, 1986.
- [29] S.Alexander. *Phys.Rev.* **B40**,7953, 1989.

- [30] A.A.Gurtovenko and A.Blumen. *Adv.Polym.Sci.* **182**, 171, 2005.
- [31] U.C. Tauber. *Critical Dynamics*, page 137. Cambridge University Press, 2014.
- [32] P.Cvitanovic R.Artuso and B.G.Kenny. *Phys.Rev.* **A39**,268, 1989.
- [33] V.G.Benza and V.Callegaro. *J.Phys.A:Math.Gen.* **23**,L841, 1990.
- [34] V.G.Benza. *Europhys.Lett.* **8**,321, 1988.
- [35] D.Nelson, T.Piran, and S.Weinberg eds. *Statistical Mechanics of Membranes and Surfaces 2nd. Edition.* World Scientific, 2004.
- [36] A.Javer, Z.Long, E.Nugent, M.Grisi, K.Siriwatwetchakul, K.D.Dorfman, P.Cicuta, and M.Cosentino Lagomarsino. *Nat.Commun.* **4**,3003, 2013.
- [37] P.G.Harper. *Proc. Phys.Soc.* **A68**,874, 1955.
- [38] M.Wilkinson. *Proc.of the Royal Soc.London* **A 391**,305, 1984.
- [39] R.Mosseri M.Duneau and C.Oguey. *J.of Phys.A:Math.Gen.* **22**,4549, 1989.
- [40] C.Sire B.Passaro and V.G.Benza. *Phys.Rev.* **B 46**,13751, 1992.
- [41] M.Widom. *Philos.Magaz.***88**,13-15,2339, 2008.
- [42] A. Zidovska, A.J. Weitz, and T.J. Mitchison. *Proc.Natl.Acad.Sci. USA*, **110**(39),15555, 2013.